LOI12-16-009

Timelike Compton Scattering on a Transversely Polarized Proton Target in SoLID

June 6, 2016

D. Keller (Contact), S. Liuti, D. Day, D. Crabb, M. Yurov, A. Rajan
University of Virginia, Charlottesville, Va

Abstract

This letter of intent is to express interest to carry out measurements of the Timelike Compton Scattering (TCS) spin asymmetries with a transversely polarized NH_3 target as a run group proposal using the Hall A large acceptance solenoid spectrometer (SoLID). The data for TCS can be taken at the same time as data taken for the Single target Spin Asymmetries (SSA) from semi-inclusive electroproduction of charged pions from a transversely polarized NH_3 target in Deep-Inelastic-Scattering kinematics using 11 and 8.8 GeV electron beams (E12-11-108). The large angle coverage and high acceptance of SolID will give very considerable more information to compliment the already proposed Timelike Compton Scattering with CLAS12 at 11 GeV while also adding additional control to systematic uncertainties in extracting different the asymmetries. The TCS with a transversely polarized target and a longitudinally polarized electron beam can be used to study the imaginary and real part of $\tilde{H}$ and E. We intend to run simultaneously on the already approved E12-11-108 experiment using 120 days of beam time at incident beam energies of 11 and 8.8 GeV and at a beam current of 100 nA.

Contents

1 Introduction

Deeply Virtual Compton Scattering (DVCS) is the simplest and cleanest way to access the Generalized Parton Distributions (GPDs) of the nucleon. The leading-twist formalism is well established for DVCS at the leading and next-to-leading orders in the strong coupling constant, and power-suppressed corrections are currently being analyzed and estimated. The DVCS process interferes with the Bethe-Heitler process resulting in an indirect access to the DVCS amplitudes. The inverse process of DVCS is time-like Compton scattering (TCS), or lepton pair production from a real photon scattering off the nucleon. In this scattering process the hard scale is provided by the virtuality of the final-state photon producing the lepton pair, which is now time-like. TCS provides an additional route to constrain GPDs [1] owing to the fact that the QCD factorization theorems leading to the handbag reaction mechanism can be proven in a similar way as for DVCS. Various dedicated experiments during a period of intense theoretical activity in the past two decades have lead us to optimize the experimental setups to best extract GPDs from DVCS through the observables known as the the Compton Form Factors (CFFs). The experimental precision attainable with the SolID detector will allow us to pursue a clear phenomenological approach where various GPD observables from different experiments can be extracted and connected to one another.

A careful analysis in terms of helicity amplitudes shows that at leading order, DVCS and TCS can be described in terms of similar combinations of GPDs. At NLO in α_S the corrections to both the quark handbag diagrams and the diagrams involving gluon GPDs will, however, be different for the two processes [2, 3, 4, 5, 6]. Similarly, the $\mathcal{O}(1/Q)$, twist three suppressed terms, where Q is the relevant hard scale, will differ in the TCS and DVCS cross sections. Accurate measurements of TCS in a wide kinematic range which partially overlaps with the DVCS regime can therefore provide a unique benchmark for understanding the dynamics of the various approximations used in the formalism for deeply virtual exclusive processes and affecting both the leading and next to leading order GPD extraction. DVCS, TCS and also Double DVCS (DDVCS), or lepton pair electroproduction can, in fact, be simultaneously expressed in a well defined theoretical framework where factorization is proven to all orders in α_S. On the contrary, for many other processes including for instance Drell Yan pair production, or meson electroproduction, QCD factorization is on a less certain theoretical standing. The accurate comparison of DVCS and TCS data afforded by the SolID detector, by providing an experimental validation of the universality and factorization properties for GPDs, will allow us to fully use the predictive power of QCD to map out the same types of GPDs at a given order in α_S and twist from different experiments. Such a validation is fundamental for creating a comprehensive database with highly enhanced statistics for both the extracted Compton Form Factors and GPDs.

The phenomenology of TCS offers in addition, straightforward access to the real part of the CFFs through the interference between the Compton and Bethe-Heitler (BH) amplitudes, using an unpolarized photon beam. The imaginary part of the CFF is also accessible using a circularly polarized photon beam. These contributions will be studies where both the four-fold differential cross section and the cosine and sine moments of the weighted cross section will be measured over a wide range of the four momentum

transfer squared, $-t$, for invariant mass of the outgoing electron pair, Q'^2 up to 9 GeV^2. Unpolarized photons, using a helicity-averaged electron beam, will be used to access the real part of the CFFs while a longitudinally polarized electron beam, producing circularly polarized photons, will be used to access the imaginary part.

The use of a transversely polarized target will be essential for isolating, in particular, the real and imaginary parts of the GPD E which is key for our interpretation of the proton angular momentum sum rule. Furthermore, it has recently become clear that the theoretical interpretation of partonic orbital angular momentum involves measurements of twist three GPDs [7, 8, 9, 10, 11]. Two distinct sets of twist three GPDs appear in the description of a proton target: four helicity conserving and four helicity flip. While the helicity conserving ones describe quark orbital angular momentum, the helicity flip ones, which require a transversely polarized target for their measurement, can be interpreted as generalizations of the twist three quark-gluon-quark correlation already appearing in the transverse polarized structure function, g_2. Although very few model predictions exist to date of the twist three GPDs, their contribution to both DVCS and TCS can be singled out precisely in experiment, since it is associated with specific azimuthal angle modulations [10]. Pioneering analyses of HERMES data show for instance, that the twist three, $\sin 2\phi$, modulation in the DVCS-BH term is sizable. The accuracy and kinematical coverage available from SolID are ideal to study these important contributions to the proton spin puzzle.

1.1 The Phenomenology of TCS

TCS, or the photoproduction of a high invariant mass lepton pair on the nucleon, is part of the family of Compton processes including DVCS and DDVCS which can be used to gain access to the GPDs in the cleanest way, *i.e.* consistently with the factorization theorems of QCD. In DVCS an electron scatters off a proton with a photon detected along with the recoil proton; TCS describes photon proton scattering where the particles detected in the final state are a lepton pair and the recoil proton; in DDVCS both photons are virtual in that a lepton pair is detected from electron scattering off the proton. For all of these processes at least one virtual photon with large four-momentum squared is exchanged between the lepton and the hadron vertices. In the kinematic regime where the four-momentum is much larger than the other mass scales, namely the proton mass and the four-momentum transfer squared between the initial and final protons t, one can write the cross section for the Compton processes in a factorized form containing the elements forming the fundamental partonic structures –the Compton Form Factors (CFFs). The latter can be written as convolutions of GPDs over the (unmeasured) longitudinal momentum fraction variable.

Similarly to DVCS, the cross section for TCS contains a BH, a pure TCS and a BH TCS interference term (Figure 1). TCS is measured in the region of large invariant mass of the outgoing lepton pair, where also an interference with the Bethe-Heitler radiation occurs, according to the reaction,

$$\gamma(q, \Lambda_\gamma) + p(p, \Lambda) \to l^-(k, h) + l^+(k', h) + +p'(p', \Lambda') \tag{1}$$

with indicated momenta and helicities. The TCS amplitudes depend on the kinematic

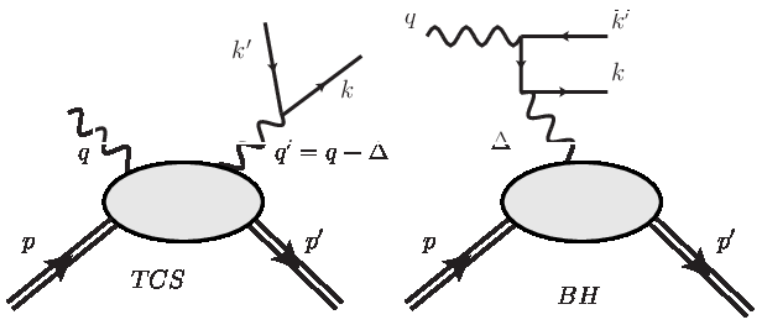

Figure 1: Exclusive photoproduction of a lepton pair through the TCS and BH processes (the crossed channels are not shown in the figure).

invariants:

$$q'^2 = Q'^2 = (k+k')^2 > 0,$$
$$s = (p+q)^2,$$
$$t = \Delta^2 = (p-p')^2 = (p'-p)^2,$$

with $q'^2 = Q'^2$ being the virtuality of the final-state photon, s being the invariant photon-proton energy squared, and t is the four-momentum transfer squared between the incoming and outgoing protons. The cross section also depends on the angles θ and ϕ associated with the final-state lepton pair. In the l^+l^- center-of-mass frame, θ is the angle between the momenta of the lepton and the recoiling proton, and ϕ is the angle between the reaction plane and the lepton decay plane. If the final-state lepton pair from this process originates from a time-like virtual photon which is emitted from a quark of the target nucleon for large enough virtuality, the amplitude of the TCS process can then be expressed as a function of GPDs. Similarly to DVCS, a pure QED, Bethe-Heitler (BH) process in which the final-state lepton pair originates directly from the initial photon of the beam is present. The TCS and BH amplitudes interfere. In JLab 12 GeV kinematics, where the BH cross section is significantly larger than the TCS cross section, one can take advantage of this interference to enhance the TCS signal [2].

The cross section is given by,

$$\frac{d^5\sigma}{dQ'^2 d|t| d\phi d(\cos\theta)} = \frac{\alpha^3}{16\pi^2(s-M^2)^2}|T|^2 \,, \tag{2}$$

where α is the electromagnetic fine structure constant, and M is the mass of the target. T is a coherent superposition of the TCS and Bethe-Heitler amplitudes,

$$T(k,p,k',q',p') = T_{TCS}(k,p,k',q',p') + T_{BH}(k,p,k',q',p'), \tag{3}$$

yielding,

$$|T|^2 = |T_{\rm BH} + T_{\rm TCS}|^2 = |T_{\rm BH}|^2 + |T_{\rm TCS}|^2 + \mathcal{I} \,. \tag{4}$$

$$\mathcal{I} \;=\; T^*_{BH}T_{TCS} + T^*_{TCS}T_{BH}. \tag{5}$$

In the one photon exchange approximation the leptonic parts for the TCS and BH respectively are,

$$\text{(TCS)} \quad \gamma^*(q') \to l^-(k) + l^+(k') \tag{6}$$

where $q'^2 = Q'^2 > 0$, and

$$\text{(BH)} \quad \gamma(q) \to l^-(k) + l^+(k') + \gamma^*(\Delta), \tag{7}$$

where $q^2 = 0$, and $\Delta^2 = t$. The corresponding amplitudes read,

$$T_{TCS} \;=\; \frac{e^3}{Q^2}\left[\overline{u}(k)\gamma_\nu v(k')\right] T_{\mu\nu}\epsilon^\mu(q) \tag{8}$$

$$T_{BH} \;=\; \frac{e^3}{\Delta^2}\left[\epsilon^\mu(q) L_{\mu\nu}(k,k',q')\right] \overline{U}(p')\Gamma_\nu U(p) \tag{9}$$

where the quantities in brackets denote the leptonic processes. $T_{\mu\nu}$ is the TCS hadronic tensor, Γ_ν describes the proton scattering vertex in BH.

1.2 TCS Formalism

The helicity dependence of the two types of amplitudes can be made explicit in the one photon exchange approximation, by expressing them as,

$$T^{h\Lambda_\gamma}_{TCS,\Lambda\Lambda'}(k,p,k',q',p') = \frac{1}{Q^2}\sum_{\Lambda'_\gamma} A^{\Lambda'_\gamma}_h(k,k',q) M^{\Lambda_\gamma,\Lambda'_\gamma}_{\Lambda,\Lambda'}(q,p,q',p') \tag{10}$$

$$T^{h\Lambda_\gamma}_{BH,\Lambda,\Lambda'}(k,p,k',q',p') = \frac{1}{\Delta^2}\sum_{\tilde{\Lambda}'_\gamma} B^{\tilde{\Lambda}'_\gamma}_{h,\Lambda'_\gamma}(k,k',q') J^{\tilde{\Lambda}'_\gamma}_{\Lambda\Lambda'}(p,p') \tag{11}$$

where we denote the electron helicity as h, the initial (final) proton helicities as $\Lambda(\Lambda')$, the initial photon helicity as Λ_γ and the final (virtual) photon helicity as Λ'_γ for TCS, and $\tilde{\Lambda}'_\gamma$ for BH. $A^{\Lambda'_\gamma}_h$ corresponds to the lepton-photon interaction in Eq.(6) and Fig.1 (left),

$$A^{\Lambda'_\gamma}_h(k,k',q) = \frac{1}{Q^2}\bar{u}(k,h)\gamma^\mu v(k',-h)[\epsilon^{\Lambda'_\gamma}_\mu(q')]^*, \tag{12}$$

$B^{\tilde{\Lambda}'_\gamma}_{h,\Lambda'_\gamma}$ corresponds to the QED process in Eq.(7), Fig.1 (right),

$$B^{\tilde{\Lambda}'_\gamma}_{h,\Lambda'_\gamma} = L^h_{\mu\,\nu}\epsilon^\mu(q) = \bar{u}(k,h)\left[\gamma^\mu(\not{q}-\not{k})\gamma^\nu\frac{1}{(q-k)^2} + \gamma^\nu(\not{q}-\not{k}')\gamma^\mu\frac{1}{(q-k')^2}\right]v(k',-h)\epsilon_\mu(q). \tag{13}$$

The hadronic components are described for TCS by $M^{\Lambda^*_\gamma,\Lambda'_\gamma}_{\Lambda,\Lambda'}(q,p,q',p')$, the helicity amplitude for the scattering process,

$$\text{(TCS)} \quad \gamma(q) + p \to \gamma^*(q') + p', \tag{14}$$

namely,

$$M^{\Lambda_\gamma,\Lambda'_\gamma}_{\Lambda,\Lambda'}(q,p,q',p') = T_{\mu\nu}\epsilon^\mu_{\Lambda_\gamma}(q)\epsilon^{*\nu}_{\Lambda'_\gamma}(q'), \tag{15}$$

whereas for the BH process $J^{\tilde{\Lambda}'_\gamma}_{\Lambda\Lambda'}$ describes the helicity structure of the hadronic vertex,

$$\text{(BH)} \quad \gamma^*(q) + p \to p', \tag{16}$$

as,

$$J^{\tilde{\Lambda}'_\gamma}_{\Lambda\Lambda'}(p,p') = \overline{U}(p',\Lambda')\Gamma_\nu U(p,\Lambda)\left(\epsilon^{\tilde{\Lambda}'_\gamma}\right)^{\nu\,*}, \tag{17}$$

where the electromagnetic nucleon current is,

$$\overline{U}(p',\Lambda')\Gamma_\nu U(p,\Lambda) = \overline{U}(p',\Lambda')\left[(F_1(-\Delta^2)+F_2(-\Delta^2))\gamma^\nu - \frac{(p+p')^\nu}{2M}F_2(-\Delta^2)\right]U(p,\Lambda) \tag{18}$$

F_1 and F_2 being the Dirac and Pauli form factors. The helicity amplitudes $M^{\Lambda_\gamma,\Lambda'_\gamma}_{\Lambda,\Lambda'}$ are written in terms of CFFs containing GPDs, in an analogous way as for DVCS. In TCS we are interested in measuring the interference term, $\mathcal{I}$, since the pure TCS is affected by a larger kinematical suppression than in DVCS [2]. The observables for a clean extraction of this term are various Single Spin Asymmtries (SSA) defined as [12],

- linearly polarized photon, unpolarized target, A_{lU}
- circularly polarized photon, unpolarized target, $A_{\odot U}$
- unpolarized beam, transversely polarized target
- unpolarized beam, longitudinally polarized target

In addition, one can form the double polarization spin asymmetries in which both the beam and target are polarized. While explicit calculations have been performed evaluating the explicit contributions to $\mathcal{I}$ in terms of the various chiral even GPDs, we limit our discussion here to two essential observations which affect the current status of GPD analyses:
1) It is important to understand the size and impact of the NLO in α_S corrections which have been predicted to be larger than in DVCS.
2) It is important to understand the inverse power corrections in the hard scale of the process which are of both kinematical origin (target mass corrections, proportional to both M^2/Q^2, and t/Q^2), and dynamical, *i.e.* twist three and twist four contributions. Twist three contributions, in particular, uniquely appear as coefficients of higher order azymuthal angular modulations. The alternative handle provided by TCS, is fundamental for clarifying these issues.

1.3 Transverse Target Observables for TCS

The availability of a transversely polarized target will allow us to single out both the GPD E and the spin flip twist three contributions, which can be considered the off-forward extension of the transverse spin structure function, g_2. Two GPDs with vector coupling and two with axial vector can be singled out, namely H_{2T} and $\tilde{H}_{2T}$ (vector) and H'_{2T} and $\tilde{H}'_{2T}$ (axial vector), according to the naming scheme of Ref.[13]. Information on both the size of these quantities and on their dependence on the various kinematical variables will provide fundamental steps for understanding the quark orbital component of the proton spin.

2 Measurements of TCS

An initial analysis for TCS on unpolarized proton target with a 6-GeV electron beam was carried out by the CLAS collaboration [15]. An additional run with high statistics of the same measurements at 12 GeV with CLAS12 is also proposed [16]. The initial Jlab studies of TCS using real tagged and quasi-real untagged photons were carried out using data previously taken in CLAS runs [15, 17]. The extractions looked at, R, the cosine moment of the weighted cross section normalized to the total weighted cross section and compared it to the theory. Several CLAS data sets with quasi-real photons (e1-6, e1f) have been analyzed and quantity R sensitive to TCS and BH interference amplitude extracted from asymmetry of azimuthal angular distribution.

The SoLID experiment E12-12-006A [18] and the suggested run of this letter builds upon experience gained from the analysis of CLAS 6 GeV data, which has established the technique for carrying out exclusive photoproduction experiments with quasi-real photons that are quite relevant for the effort here.

The results from the above analysis can be compared with an TCS analysis using the g12 data set [17], which was the only 6 GeV energy CLAS data set with tagged real photons. In addition to demonstrating the feasibility of the proposed measurement, the pilot experiments at 6 GeV stimulated the development of new analysis methods. An example of this was the introduction of the cosine moment R, evaluated within the acceptance of the detector in the $\phi_{CM} - \theta_{CM}$ plane. Whereas the original definition of R implies using the integration ranges corresponding to the detector acceptance, R adds an function a $\phi_{CM} - \theta_{CM}$ for a given kinematic bin.

Despite the usefulness of the 6 GeV data for developing the TCS program, only the 12 GeV era will provide the required luminosity and kinematic coverage. In particular, the higher beam energy will make it possible to study a range of invariant lepton pair masses where there are no meson resonances that complicate the interpretation of the measurement. Only data above the ϕ mass were used for TCS analysis at 6 GeV, but at 12 GeV it will be possible to move this range above the mass of the ρ'.

There will be a proposal (LOI12-15-007) in Hall C which we hope can use a pure photon source and two Neutral Photon Spectrometers to precisely measure some select kinematics. This measurement will add two more independent (single, double) asymmetries with a transversely polarized target enabling the extraction of $\mathrm{Im}(E)$ through the transverse spin physics. This data will add new degree of freedom in GPD models at leading twist and leading order, independent from all current DVCS measurement. If we assuming GPD universality, we can also extract most of the Compton Form Factors (CFF) at the same time using combined DVCS+TCS fits, bringing new constraints to the GPD models.

This LOI suggested parasitic run for transversely polarized TCS will add considerable kinematic coverage for the transverse target single and double asymmetries using the large acceptance of SoLID. This makes these two efforts very complimentary.

One of the measured observables for the suggested experiment is the single target spin asymmetry. The transverse target spin asymmetries are sensitive to the imaginary part of the amplitudes and and the BH are very well understood allowing for clean extraction of the TCS amplitude and direct relation to the GPD parameterization. We expect a ϕ modulation for the transverse components of the asymmetry. This leads to a kinematic

sensitivity to the GPDs H, $\tilde{H}$, and E.

Double spin asymmetries with a circularly polarized beam are sensitive to the real part of the amplitudes. Since BH alone gives non-zero asymmetries so a good understanding of the BH amplitude is required. These asymmetries are, however, sensitive to the GPDs, and once the experimental procedure is demonstrated, they could provide a strong constraint on the GPD fits. The t and ϕ dependence of these asymmetries are presently being investigated and new predictions will be investigated soon.

3 The Run Group Experiment

3.1 Overview

We express interest to study the photoproduciton of lepton pairs, $\gamma p \to l^+ l^- p'$, in a wide range of kinematics using the SoLID detector in Hall A and a 8.8 and 11 GeV longitudinally polarized electron beam impinging on a transversely polarized proton target. The fully exclusive reaction $ep \to e^+ e^- p'(e')$ with the undetected electron (e') scattering at small angle. The quasi-real (along with some real) photoproduction of TCS in data will be extracted using the detected lepton pair and the recoil proton and deducing the scattered electron from the missing-particle kinematics.

The multiple final state particle detection in wide kinematics along with the need for large ϕ modulation with high luminosity and large acceptance makes SoLID the ideal detector system for the measurement. The SoLID experiment E12-11-108 [19] to measure the target single spin asymmetry in semi-Inclusive deep-inelastic reaction on a transversely polarized proton contains all the needed equipment to detect the TCS final states e^+e^-p. It is possible to have a common trigger as E12-11-108 using the detected electrons with data being collected in parallel. The same target will be used which is a 3 cm long upgraded NH_3 target transversely polarized in Hall A with a 100 nA electron beam with energies of 8.8 and 11 GeV.

3.2 The experimental observable

In this experiment, we will form the target transversely polarized asymmetry A_{Ui} (where i stands for x and y) as well as the double spin asymmetry with a circularly polarized beam and a transversely polarized target,

$$A^h_{Ui} = \frac{\sigma^+ - \sigma^-}{\sigma^+ + \sigma^-} \tag{19}$$

where $\sigma^\pm$ for the 4-differential cross section $\frac{d^4\sigma}{dQ'^2 dt d\Omega}$, and the $\pm$ indicate the direction of the polarization vectors.

The double spin asymmetries are defined as,

$$A^h_{\circ i} = \frac{\sigma^{++} + \sigma^{--}) - (\sigma^{+-} + \sigma^{-+}}{\sigma^{++} + \sigma^{--} + \sigma^{+-} + \sigma^{-+}} \tag{20}$$

where $\sigma^{\pm\pm}$ represents the 4-differential cross section $\frac{d^4\sigma}{dQ'^2 dt d\Omega}$, i is the target polarization index and $\circ$ represents the polarization index of the beam.

3.3 Detector System

We now discribe some of the details of the detector systems which comes directly from the approved proposal [19] with some updates from the target sections. The entire detector system consists of two parts: forward-angle detectors and large-angle detectors. The polar angle coverage for the forward-angle detectors is from 9° to 14.3° and the momentum coverage is from 1.0 GeV/c to 7.0 GeV/c. The total solid angle is about 80 msr for this

momentum coverage. GEM detectors will be used as tracking detectors (Six layers of the GEM detectors are placed inside the coils. Five of them will be used in tracking for the forward-angle detection). A combination of an electromagnetic calorimeter, gas Cerenkov counters, a layer of Multi-gap Resistive Plate Chamber (MRPC) and a thin layer of scintillator will be used for particle identifications. Although, a 3-bounce Cerenkov geometry is shown in Fig. 2, we plan to use a 1-bounce geometry for the gas Cerenkov. The polar angle coverage for the large-angle detectors is from 17° to 24° which provides additional 160 msr solid angle. They are mainly used for electron detection for a momentum range of 3.5-8.0 GeV/c. The expected π/e ratio is smaller than 1.5. The shashlyk-type calorimeter proposed originally to PAC 35 [20] will be sufficient to provide the pion rejection (200:1). Most recent studies show that a calorimeter based on scintillator fiber (SciFi) technique is also viable. Currently, more detailed studies of performance and cost for both options are ongoing. Four layers of GEM detectors will be used as tracking detectors. The total solid angle is about 240 msr for this momentum range.

We plan to use the JLab/UVa/SLAC polarized NH_3 target with an upgrade. The polarized NH_3 target has been successfully used in several experiments in Hall C (SANE, RSS and Gen) and at SLAC (E143, E155 and E155x). The target is currently being installed in Hall A for the g2p/GEp experiments, which are scheduled to run from November, 2011 to May 2012. The target is based on the principle of dynamic nuclear polarization (DNP) by using microwave pumping to reach high proton polarizations. The target is operating at a low temperature of 1 K and a strong magnetic field of 5 T. The NH_3 material is chosen because of its proven property of excellent radiation-resistance to electron beam damage to the target polarization. The current achieved best performance for double-polarization experiments with a polarized lepton beam on a polarized proton target was with this target reaching a polarized luminosity of 10^{35} proton/cm^2/s with an in-beam polarization of 80%. Details of the target are described in Sec. 3.4.

A solenoid spectrometer (Solenoidal Large Intensity Device (SoLID)) was proposed for three approved experiments. These include a 11 GeV PVDIS experiment [21], and two SIDIS experiments [20, 22, 23]. Several solenoids with a bore diameter of about 3 m and central field of about 1.5 T have been used in recent experiments (see Table. 3.3). The best magnet option is the BABAR maget. In this letter, we mostly consider the BABAR solenoid [24], but it will be very similar if we use the Cleo-II magnet, and the kinematic coverage will be reduced by about 20% were the CDF magnet used.

Experiment	B (Tesla)	Bore D (m)	Length (m)	MJ	X_0
BaBar	1.5	2.8	3.46	27	<1.4
Cleo-II	1.5	2.9	3.8	25	2.5
CDF	1.5	2.90	5.00	30	0.85

Table 1: Parameters of recently used solenoidal magnets.

The TCS cross section is measured in combination with the much larger Bethe-Heitler (BH) cross section with which it interferes, the rate estimates for TCS are based on the BH cross section as given in [25].

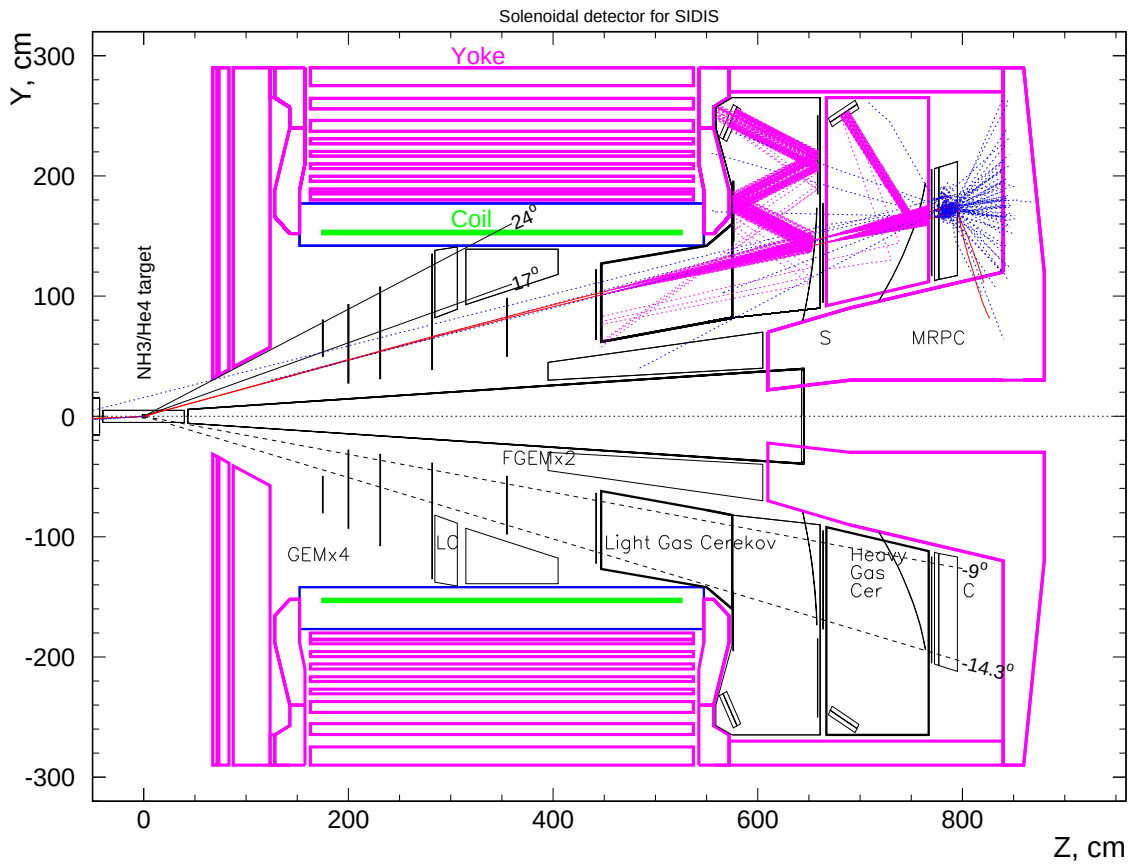

Figure 2: The experimental layout of the SoLID with a polarized NH_3 target. For forward angle detection, there are five layers of GEM detectors ("FGEM") inside the coils in the upstream of the Gas Čerenkov. A 2 m long light Gas Čerenkov is used to separate the electrons and pions. A heavy gas Čerenkov ("HG", 50 cm long) is placed after the light gas Čerenkov to exclude the kaons and the protons from the pions. The shower detector ("S") will be used to provide the trigger, coincidence timing and additional electron/pion separation, especially at high momentum. For the large angle detector, four layers of the GEM detectors ("LGEM") are placed inside the coils. A "shashlyk"-type calorimeter ("LS") will be used to provide trigger, coincidence timing and electron/pion separation.

3.4 Polarized NH_3 target

We propose to us an upgraded version of the JLab/UVa/SLAC polarized NH3 target. The main upgrade will be to use a new magnet to replace the aging Helmholtz-coil magnet and to have fast spin-flip capability with the AFP technique. The target is based on the principle of dynamic nuclear polarization (DNP) by using microwave pumping to reach high proton polarizations [26, 27].

The target is operating at a low temperature of 1 K and a strong magnetic field of 5 T. The NH3 material is chosen because of its proven property of excellent radiation-resistance to electron beam damage to the target polarization. The current achieved best performance for such kind of experiments with a polarized lepton-beam on a polarized proton target was with this target which reached a luminosity of 10^{35} proton/cm^2/s with an in-beam average polarization of 80%. In this experiment, the ability to flip the target polarization frequently is important for the suggested measurements in terms of reducing systematics. Adiabatic fast passage (AFP) NMR has been demonstrated as an effective (90% efficiency) way of spin flip for a DNP target with ^{7}LiH as a target material [28] and recently a AFP spin flip test has been achieved by the UVA polarized target group for NH_3 with approximately 52% efficiency for the condition at 5T/1K confirming predictions ([29]). It is expected that efficiency can be still improve by optimizing the Q-value of the circuit which is sensitive to the coil geometry and amount of material. The AFP results already indicate that 20 minutes could potentially be safe for every target helicity change.

A set of superconducting Helmholtz coils provide a 5-T field with a highly uniform area, about 3 cm $\times$ 3 cm $\times$ 3 cm in the center. The existing magnet was designed mainly for longitudinal polarization while also allowing transverse polarization. In the longitudinal case, it has a large opening in the forward region ($\pm 45°$) for scattered particles to be able to reach the spectrometer/detector system, while in the transverse case, it has only about $\pm 17°$ nominal opening in the forward region. The new design will optimize to allow both transverse and longitudinal to have a nominal forward opening of more than $\pm 28°$, while maintain the same maximum field and uniform field region in the center.

A couple of target cells with length of 3 cm are immersed in a vessel filled with liquid helium which was maintained at 1 K by a series of large pumping system. The target cell is filled with beads of solid NH3 material with a typical packing factor of about 50% with the rest of the space filled with helium.

The target material is usually prepared by irradiation before-hand at a low energy electron facility, such as NIST. During the experiment, the target material is exposed to 140 GHz microwaves to drive the hyperfine transition which aligns the proton spins. The DNP technique produces proton polarizations of greater than 90% in the NH3 target. The heating of the target by the beam causes a drop of a few percent in the polarization, and the polarization slowly decreases with time due to radiation damage. Most of the radiation damage can be repaired by annealing the target at about 80 K, until the accumulated dose reached is greater than about 17×10^{15} e$^-$/cm^2, at which time the target material needs to be replaced.

Target polarization is measured with an NMR system, which is calibrated with a measurement of polarization in thermal equilibrium (TE). Typical precision reached in the polarization measurement is about 3% (but less than 2% for ideal test lab conditions).

To achieve highest polarization levels in dynamic nuclear polarization (DNP) experiments, target materials must be subjected to microwave irradiation at a particular frequency determined by the difference in the nuclear Larmor and electron paramagnetic resonance (EPR) frequencies. However, this resonant frequency is variable; it drifts as a result of radiation damage. Manually adjusting the frequency to accommodate for this fluctuation can be difficult, and improper adjustments negatively impact the polarization. In response to this problem, a controller has been developed which automates the process of seeking and maintaining optimal frequency. The creation of such a controller has necessitated research into the correlation between microwave frequency and corresponding polarization growth or decay rates in DNP experiments. Knowledge gained from the research of this unique relationship has additionally lead to the development of a Monte-Carlo simulation which accurately models polarization as a function of frequency and a number of other parameters. The simulation and controller continue to be refined, however, recent DNP experimentation has confirmed the controller's effectiveness.

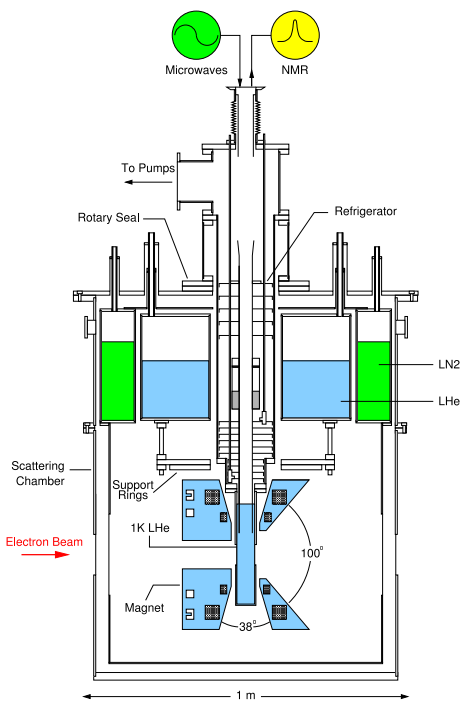

Figure 3: Polarized target system

For transverse polarization, the target field is perpendicular to the beam axis. This creates a deflection of electron beam (which is more significant for lower beam energies). To ensure proper transport of the beam, a chicane will be employed. A beam chicane system has been developed for the g2p/GEp experiments which will be more than enough to satisfy the need of this proposed experiment. Th electron beam will be pre-bended such that the outgoing beam after the target will be going straight to the regular Hall Abeam dump. No local beam dump will be necessary as in the g2p/GEp case.

To reduce the target depolarization due to beam, a large size (2.5 cm) raster system (slow-raster) will be used in addition to the existing Hall A fast-raster system. The typical beam current this target can tolerate is about 100 nA. Beam diagnostic system (beam

current and position measurement system) which can handle such a low current will be needed.

Fortunately, all of the above beam-line system has been developed and is being implemented for the upcoming g2p/GEp experiments. The beam diagnostic system is compatible with the high beam energies. Minor modifications will be needed to make the slow raster working with high beam energies.

3.5 Acceptance and Kinematic Coverage

With the target field, the polar angle coverage for electrons θ_e is from 3° to 28°. Although the current UVA/JLab polarized NH_3 target has about $\pm 16^0$ forward opening in the transverse spin configuration, the planned upgrade will have a new magnet designed to have optimized geometry for transverse polarization such that it will have forward opening of more than ±28°. The acceptance study assumed the upgraded configuration with no forward angle limitation.

The effect on the azimuthal angular coverage from the polarized NH_3 target field is significant, and has been studied by GEANT3 Monte Carlo simulation which includes realistic spectrometer models, detector geometries, and the target field [1]. A very important experimental issue associated with such a target in a strong transverse field, known as "line of flame" is clearly shown in our simulations, where extremely high backgrounds are seen in highly localized areas of the acceptance. One way to get around this issue is to "remove" certain areas of the detectors where "line of flame" passes through by turning off part of the detectors. The other way is to add collimators in the target region to block these high rate regions more efficiently. Based on previous GEANT3 studies for SoLID experiment PR12-10-014 and E12-10-006, resolutions are not an issue for the proposed experiment. Reconstruction of angles is more important which can be addressed by careful simulations of the optics before the experiment and calibration during the experiment. Optics studies based on Monte Carlo simulations have been completed recently for the g2p/GEp experiment employing also the transversely polarized NH_3 target in Hall-A, and a careful optics study with beam is being planned for the these experiments. Our proposed experiment will benefit from the experience of the upcoming g2p/GEp experiments which are scheduled to run in the fall of 2011.

[1] The exisiting SLAC/UVA/JLab NH_3 target field map is used in the GEANT3 simulations, though a new magnet optimized for the proposed experiment will be needed.

3.6 Detectors

In this experiment, we propose to use the same setup as in the approved ^{3}He SoLID SIDIS proposals [20, 22, 23] with cerntain regions of detectors disabled (or removed) for the "line of flames". In this section, we will focus on the new dedicated studies on the current setup.

3.6.1 GEM Trackers and Background Rates

A total of six GEM trackers will be used to provide the momentum, angle and interaction vertex of the detected particle. For the forward-angle detection, except for the first layer, all other layers will be used. For the large-angle detection, the first four layers of GEMs will be used, where the background rate is expected to be smaller than the forward-angle. The detector configuration is shown in Fig. 2.

The background rates on the GEM detectors were estimated using GEANT3 simulation with all the physics processes(such as Moller/Mott etc) turned on. The background simulation after removing the "line of flame" shows that the rates on the GEM chambers similar to those estimated for the ^{3}He proposal. Fig. 4 shows the results obtained from the simulation for two different beam energies (11 GeV and 8.8 GeV). The estimated background rates are much smaller than 30 KHz/mm^2, in which GEMs have been used in the COMPASS experiment. At the proposed background rates, tracking has been sucessfully demonstrated with the proposed configuration in ^{3}He proposal [20, 22, 23].

3.6.2 Expected Resolutions

The optics of the BaBar magnet is studied which includes the target field of the current UVA/JLab polarized proton target. Fig 5 shows the resolutions obtained from the simulation for different polar angles (θ), and shown as a function of momentum of the scattered particle. The interaction vertex position resolution is assumed to be 1.5 cm, which is determined by the target length. A 200 μm position resolution on GEM is assumed. The resulting momentum resolution $\frac{\delta p}{p}$ is about 1% (σ), with a larger resolution at high momentum. For angular resolution, instead of using the common polar angle θ and azimuthal angle ϕ in the lab frame, we decided to use $\frac{dx}{dz}$ and $\frac{dy}{dz}$. Here, $\frac{dx}{dz}$ is the slope of tracks in the plane perpendicular to the target holding field. $\frac{dy}{dz}$ is the slope of the tracks in the plane of the target holding field and the incident beam direction. The average $\frac{dx}{dz}$ and $\frac{dy}{dz}$ are about 0.007 and 0.0012, respectively. The main reason that the resolution on $\frac{dx}{dz}$ is much larger than $\frac{dy}{dz}$ is due to the extended target length.

Fig. 6 shows the resolutions of the kinematic variables x, Q^2, z, P_T, ϕ_s and ϕ_h, after including the resolution on momenta of the scatterted electron and the leading hadron and slopes of directions of incident electron, scattered electron and the leading hadron. The resolution in x, Q^2, z, and P_T are much smaller than the proposed bin size. Furthermore, the maximum resolution in ϕ_s and ϕ_h are 1.14° (small x) and 5.7° (small P_T), respectively. The systematic uncertainties on Collins and Sivers effect are below 0.5% (relative), assuming a resolution of 1.14° and 5.7° of ϕ_s and ϕ_h. The effect on pretzlosity is below 2.5% (relative) in comparison.

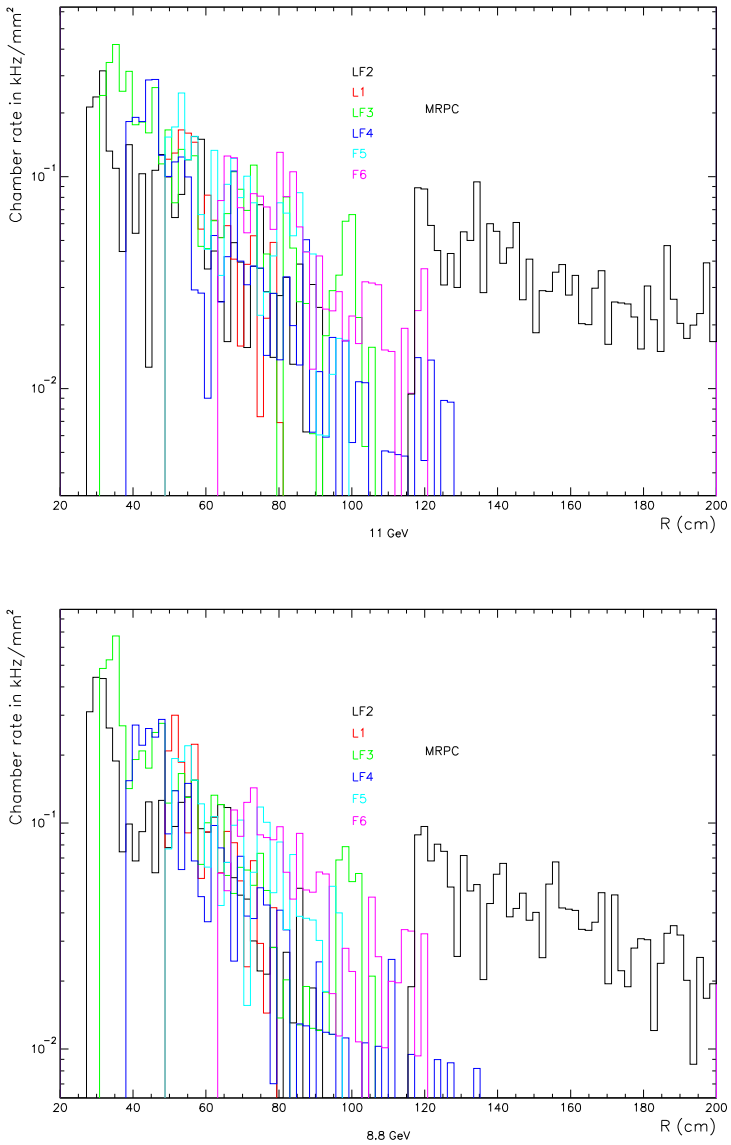

Figure 4: The simulated background for 11 (8.8) GeV beam is shown in upper (lower) panel. The rate on each GEM layer is plotted as a function of its radius. The label "L1" denotes the first layer in the large-angle. "LF2", "LF3" and "LF4" are shared between the large-angle and forward-angle detection. The "LF5" and "F6" are used in the forward-angle only.

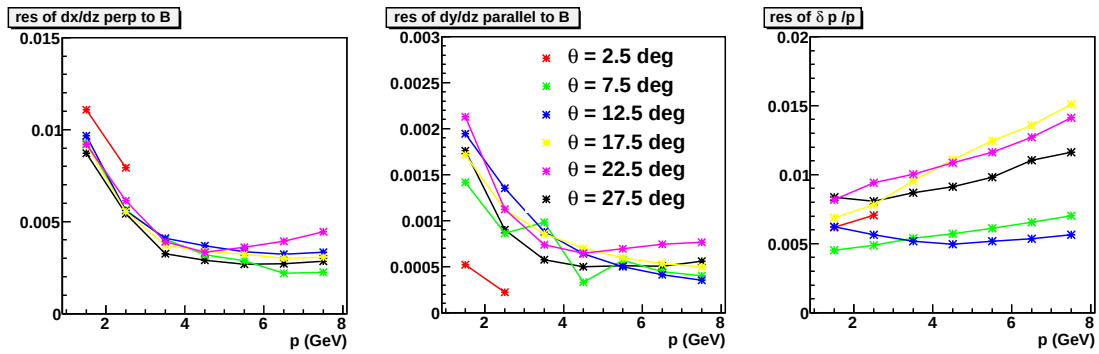

Figure 5: The resolutions of dx/dz, dy/dz and momentum. The x axis is the momentum of the particle.

3.6.3 Electromagnetic Calorimeter

A "shashlyk" type electromagnetic calorimeter will be used in both forward and larger angle to identify electrons and hadrons. The calorimeter will be split into preshower/shower type configuration, which can give a pion rejection factor of 100:1 with E > 1.0 GeV and an energy resolution of $\leq 5\%/\sqrt{E}$.

The Shashlyk type calorimeter is a sampling type calorimeter constructed from alternating layers of scintillator and heavy absorber. The scintillation light is carried to the photon detector by a wave-length shifting optical fibers running longitudinally through the calorimeter. The calorimeter design is currently being studied using a GEANT4 simulation. An optimal design is considered to reach the required goals on the pion-rejection and energy resolution. In a typical design, each layer consists of 1.5 mm thick scintillator plate and a 0.6 mm thick absorber. The effective radiation length (X_0) is about 21 mm. More details on the status of the calorimeter design can be found in the updated proposal E12-11-007 to PAC38 [23].

The background rates on the calorimeter have been calculated using the GEANT3 simulation for this experiment, and the results are shown in Fig. 7. With further optimization of the setup we can reduce the background rates on the calorimeter. Overall the background level is at most comparable to that of the approved experiments using the ^{3}He target [20, 23].

3.6.4 Particle Identification Detectors

For electron detection, a light gas Cerenkov will be used to combine the electromagnetic calorimeter system at forward angle. An E&M calorimeter will be enough to provide electron PID at large angle, where the pion/e ratio is expected to be smaller than 1.5 for particles with momentum larger than 3.5 GeV. The pion PID will be provided by a MRPC time-of-flight detector (separate from protons, and kaons at low momentum), gas Cerenkov and E&M calorimeter (separate from electrons), and a heavy gas Cerenkov (separate from kaons at high momentum). The background rate of MRPC is also simulated through GEANT3 program and shown in Fig. 4. The baseline parameters of detectors are assumed to be same as in Ref. [20, 23]. A beam test of a prototype MRPC for SoLID in Hall A is

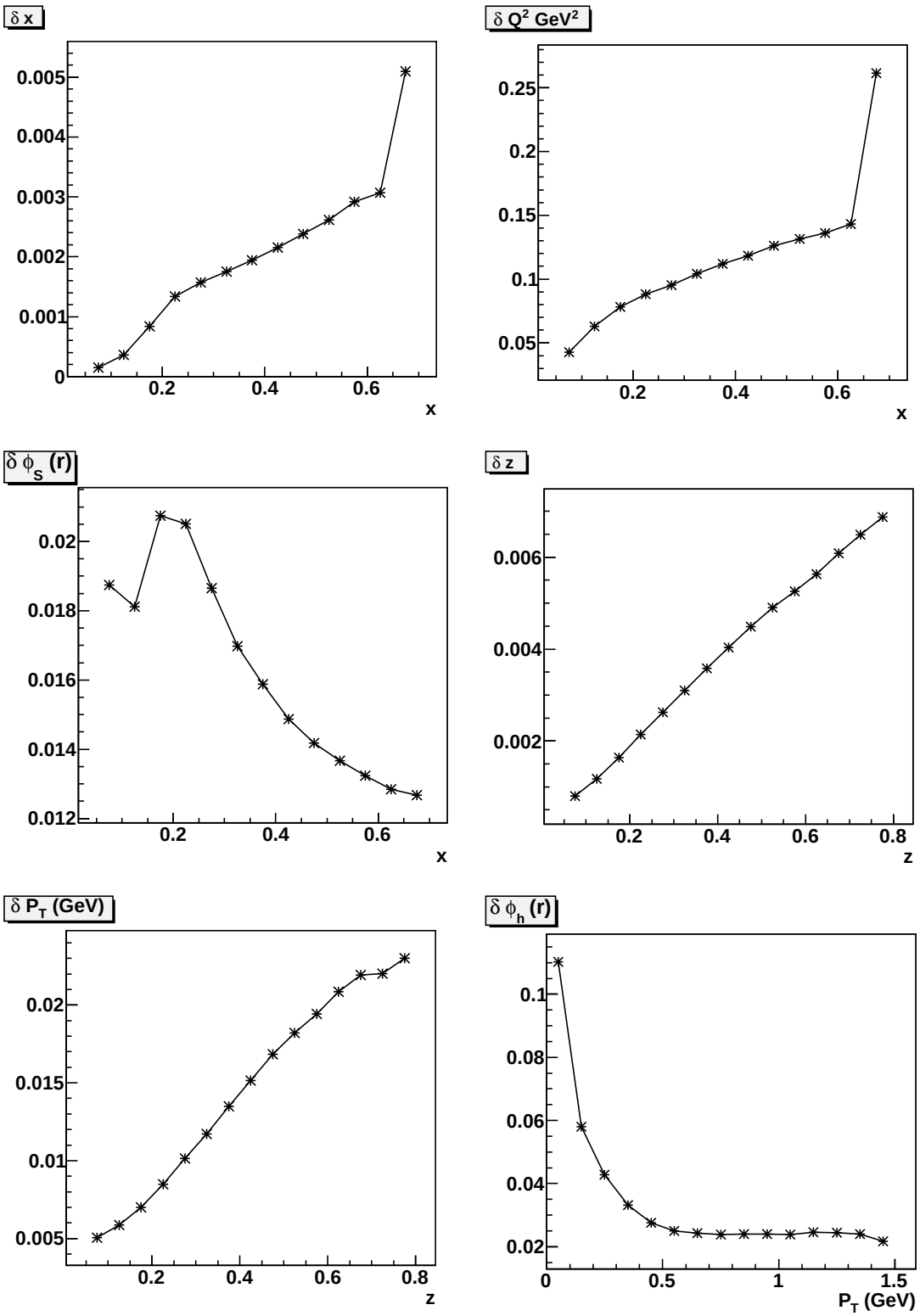

Figure 6: The resolutions of kinematic variables x, Q^2, ϕ_s, z, P_T, ϕ_h.

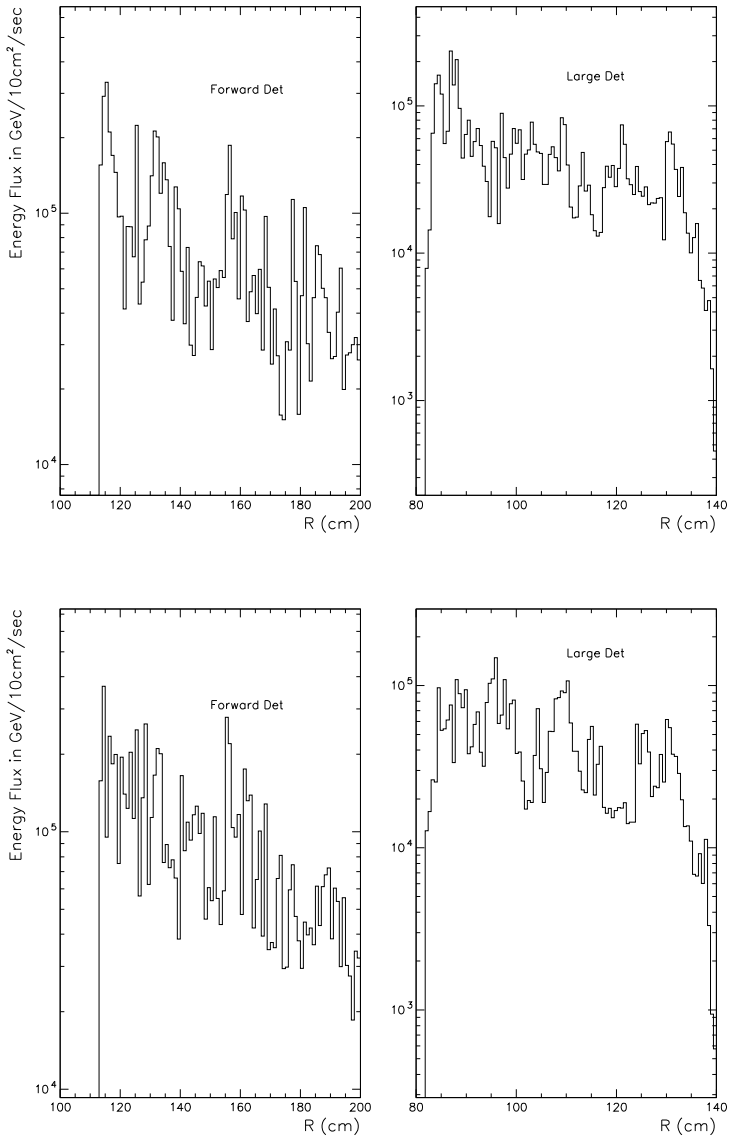

Figure 7: The energy flux (in GeV/10cm^2/sec) on the calorimeter as a function of its radius. The left (right) panel shows the background for the forward-angle (large-angle) detector.

planned for fall 2011.

3.6.5 Update on Cerenkov Detectors

This experiment requires both electron and pion detection. In order to unambiguously identify both electrons and pions several PID detectors will be required. Two Cherenkov detectors will be an essential part of the PID scheme.

Electron identification: the light-gas Cherenkov

A Cherenkov detector filled with CO_2 at 1 atm would ensure electron-pion separation up to a momentum of 4.65 GeV. This detector, extending 2.1 m along the beam line, would be positioned immediately after the SoLID coil. The close proximity to the SoLID magnet requires careful consideration of various options for the photon detectors. In addition, the detector optical system is expected to provide full coverage in the azimuthal angle.

Recently a GEANT4 simulation was used to optimize the design of the optical system. It was found that with just one system of 30 spherical mirrors (following the SoLID sectoring) near perfect collection efficiency, $> 95\%$, can be achieved with a $12''$ by $12''$ photon detector (active area). This size could be easily scaled down to $6''$ by $6''$ by employing Winston cones. A schematic of this setup is shown in Fig. 1 where Cherenkov photons (green) produced by the passage of electrons (red) through the radiator gas are reflected by 30 spherical mirrors (grey) and focused onto the photon detectors (cyan).

The one-mirror optical system is a significant improvement over the three-mirror design outlined in the proposal presented to PAC35. The Cherenkov photon yield lost due to reflections off multiple mirrors is reduced. This is particularly important for the GEM + CsI option where is technically challenging to manufacture and maintain mirrors with good reflectivity in the UV region. In addition the one-mirror design is more practical and cost efficient form the manufacturing and installation point of view.

The same GEANT4 simulation has been used to describe the photon detector response and this is yet another improvement since PAC35. Two options have been considered for the photon detectors: magnetic field resistant photomultiplier tubes, PMTs, (Fig. 1, left panel) to be used in combination with Winston cones and gaseous electron multipliers with Cesium Iodide coating, GEMs + CsI, (Fig. 1, right panel).

For the PMT option the Hamamatsu model H10966A-100 was considered. This is a $2''$ multi-anode PMT with up to 94% photocathode coverage and good quantum efficiency down to wavelengths of 200 nm. These characteristics make this model ideal for tiling and we plan to use 9 such PMTs per sector, in a 3 by 3 array, to cover a $6''$ by $6''$ area. It is fairly resistant in magnetic field: such unshielded PMT experiences up to 60% gain reduction in 100 Guass field according to data provided by Hamamatsu. This is a significant improvement when compared to a regular $5''$ PMT which,if unshielded, would experience a similar gain reduction at only 4 Gauss. To establish whether H10966A-100 could withstand the magnetic field of SoLID we plan to test it with shielding this Summer at Temple University. If the magnetic field test results are satisfactory we plan additional tests at Jefferson Lab to ensure suitability in high-background environment.

An estimate of the number of photoelectrons for this option with the configuration described above (Fig. 1, left panel) yields between 25 and 35 photoelectrons. The number

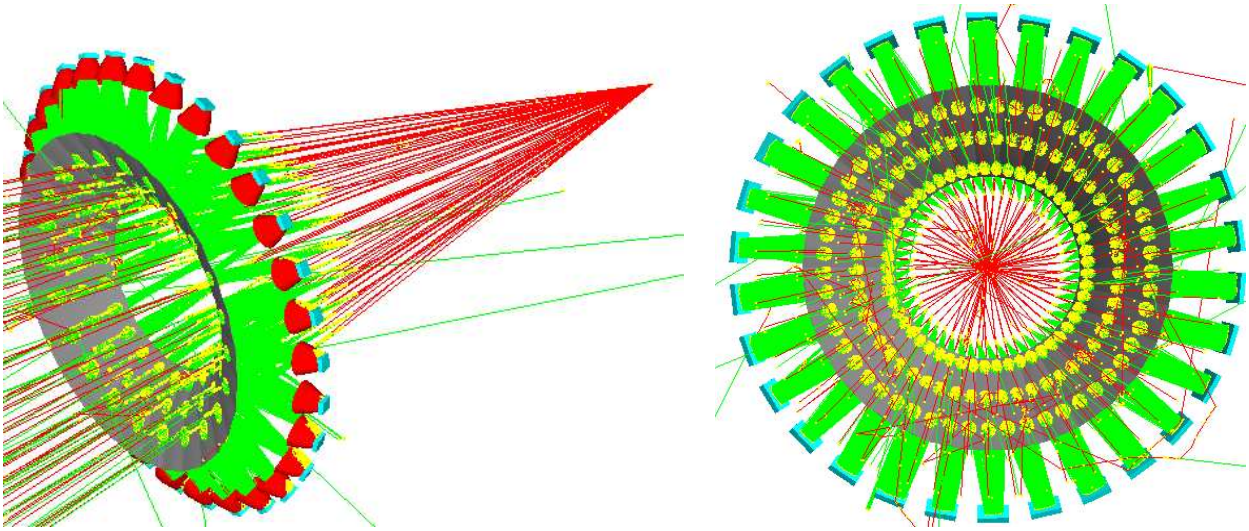

Figure 8: Setup of the light-gas Cherenkov: a system of 30 spherical mirrors (grey) will focus the Cherenkov photons (green) created by the passage of electrons (red) through a radiator gas onto photon detectors (cyan). Left panel: setup for the PMT option, side view (see text). Right panel: setup for the GEM + CsI option, back view - as seen from the beam dump (see text).

depends slightly on the electron polar angle: because of the mirror positioning in the tank electrons with higher polar angles traverse a longer path in the radiator gas than those with lower polar angles. This estimate includes wavelength dependent corrections like mirror and Winston cones reflectivities and the PMTs quantum efficiency as well as an overall correction of 0.8 to account for the reduction in the photocathode effective area as a result of tiling.

The GEM + CsI is an alternative to the PMT option and has the clear advantage of being resistant in magnetic filed. This has been used successfully as a photon detector during PHENIX experiment at BNL in a Hadron Blind Detector [31] and a similar setup is being developed in Japan for use in JPARC experiments [32]. The photon detector consists of three layers of GEMs the first being covered with CsI which acts as a photocathode. The operational regime for CsI is the ultraviolet (UV) region, between 120 and 200 nm [33]. This requires a radiator gas with good transparency in the UV and with very good purity to avoid photon absorption by impurities. Thus for the GEM + CsI option, a suitable gas choice would be CF_4 which, unlike CO_2, is transmissive between 120 nm and 200 nm [34]. This gas would still give an acceptable threshold for electron-pion separation and it was the gas of choice for the successful PHENIX run.

The number of photoelectrons for this option was estimated using the GEANT4 simulation and assuming a 12″ by 12″ photon detector (Fig. 1, right panel). A signal of 20 to 30 photoelectrons was obtained. Wavelength dependent corrections as mirror reflectivity and quantum efficiency of CsI were taken into account as well as an overall correction of 0.54 to account for loss of signal due to gas transparency, reduced photocathode coverage of the GEM (about 20% of the GEM surface is occupied by holes), transport efficiency of avalanche electrons through gas, etc.

Pion identification: the heavy-gas Cherenkov

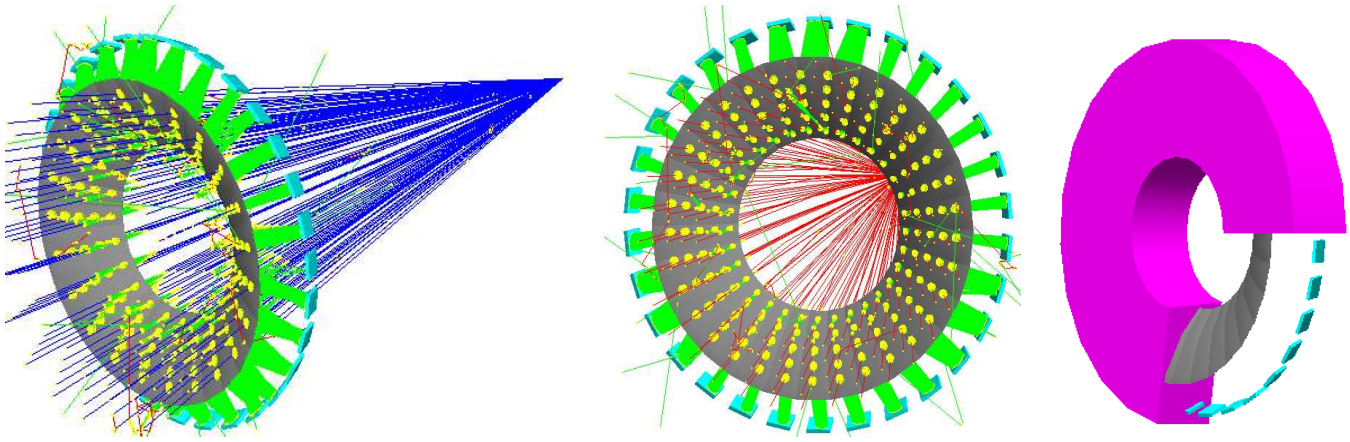

Figure 9: Optical system for the heavy-gas Cherenkov: a ring of 30 spherical mirrors (grey) will focus the Cherenkov photons (green) created by the passage of positive (left panel) and negative (center panel) pions through the C_4F_{10} radiator gas onto photon detectors (cyan). The placement of the mirrors and photon detectors in the tank (magenta) is also shown (right panel).

A Cherenkov detector filled with C_4F_{10} at 1.5 atm would be placed right after the light-gas Cherenkov to provide pion-proton/kaon separation in a momentum range from 2.2 to 7.6 GeV. A GEANT4 simulation is underway for this detector and the same design ideas and concepts will be used as for the light-gas Cherenkov.

Figure 2 displays preliminary results from this simulation: focusing of Cherenkov light with one spherical mirror is shown for both positive (left panel) and negative pions (center panel). The photon detector size is set to be 12″ by 12″ just as for the light-gas Cherenkov. With this setup the light collection efficiency is very good for the entire kinematic range of interest.

3.6.6 Trigger Setup and DAQ

The single rate in E12-12-108 will be about factor 5-10 lower than the sister experiment with a polarized ^{3}He target [20, 23]. Therefore, the design of trigger setup and DAQ of the ^{3}He experiment will satisfy our needs in this setup.

3.7 Beamline Instrumentation

3.7.1 Beam Chicane

In this experiment the polarization direction of the proton target will be held transverse to the beam direction. The strong magnetic field of the target will create a non-negligible deflection of the electron beam. To ensure the proper transport of the beam into the downstream exit beam pipe, a chicane will be employed. Two chicane magnets will be used for this purpose. The first one will be located 10m upstream of the target and this will bend the beam out of the horizontal plane to vertically down. The second magnet which will be located about 4m upstream of the target will bend back the beam at an angle that will compensate the 5 Tesla target field. We will choose the bend angle such that the beam will pass through the exit beam pipe after interacting with the target. A

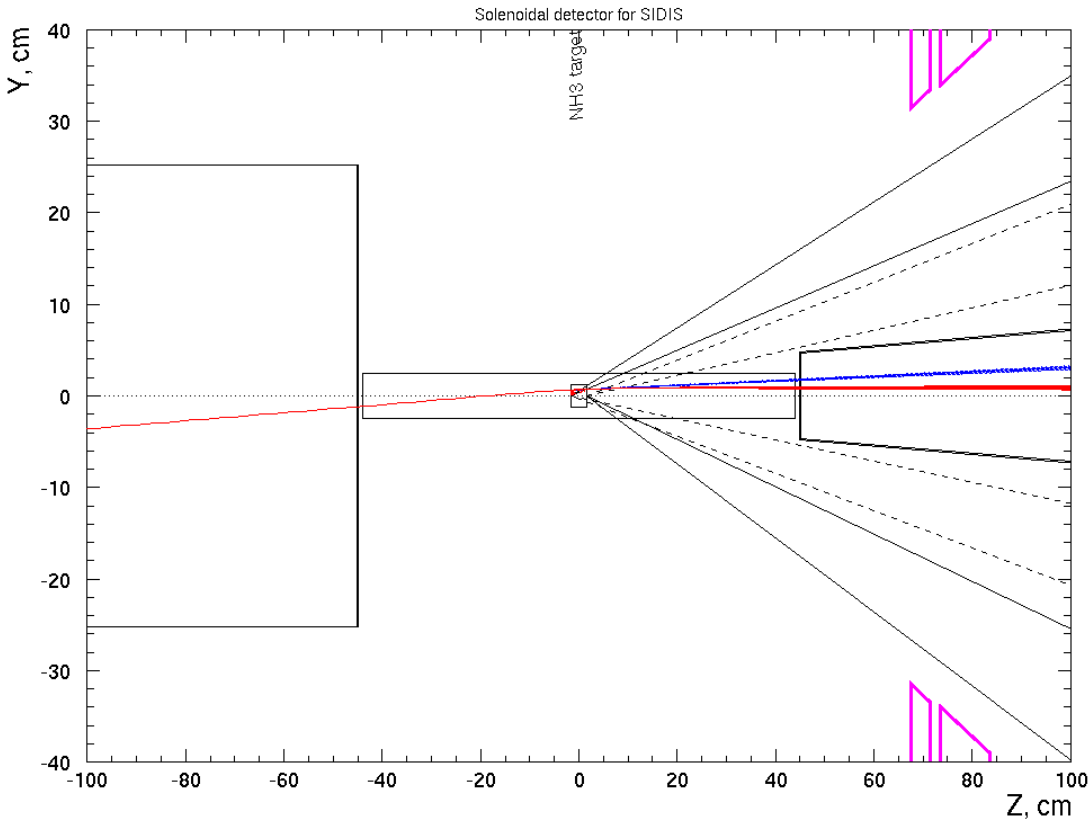

Figure 10: Event display of the beam transport at the target region with the initial bend of the beam before hitting the target. The red color denotes the 11 GeV beam and the blue color denotes the uncharged particles (mostly bremsstrahlung photons). The NH_3 target field direction is pointing into the page.

GEANT3 simulation was performed to optimize the bend angle. The simulations included physics processes such as synchrotron radiation and Bremsstrahlung. Fig. 10 shows an event display for the 11 GeV beam. Beam position monitors will be used before and after the chicane for the proper transport of the beam. They will also be used in determining the beam positions at the target.

3.7.2 Beam Charge Monitors

Typically low beam currents (up to 100 nA) are used for the polarized proton target to reduce the depolarization effects and any significant changes to the density. The standard Hall-A BCM cavities are linear down to 1 μ A. An upgrade of the beam diagnostic elements such as BCM, BPM and Harps are planned for the g2p experiment (E08-028) in Hall-A, which uses the polarized proton target, and is scheduled to run in Oct 2011. The planned upgrade will allow us to measure the beam charge and positions up to 50 nA current. In order to calibrate the beam charge a tungsten calorimeter will be used. This device is also being refurbished and will be used in Hall-A during winter 2011 running. Tungsten

calorimeter can provide an absolute calibration of Hall A BCM with an accuracy of better than 2%.

3.7.3 Slow and Fast Raster

Along with the existing Hall-A faster raster we will use a slow raster just upstream of the target. The fast raster will have a 2 mm x 2 mm pattern and the slow raster will cover a circle of 20 mm diameter. This is done in order to uniformly cover most of the surface of the target cell which has a 25 mm diameter.

4 Some Systematics

To achieve the proposed precision, it is very important to control the systematic uncertainties. The large azimuthal angular coverage plays an important role in reducing the experimental systematic uncertainties. The large signal-to-noise ratio will also help to reduce the systematic uncertainties in subtracting backgrounds.

4.1 Target spin flip

To minimize systematic uncertainty, frequent target spin reversal is necessary. Due to the strong target magnetic field (5T), it is difficult to rotate target field direction to realize the spin reversal. The practical method is to use RF spin-flip with adiabatic-fast-passage AFP technique. There was an extensive study done by Haulte et al. [38] many years ago. It was shown that with ^{7}LiH, the efficiency of AFP spin-flip reached up to 90%. ^{7}LiH, with its excellent radiation resistance and high dilution factor, could be a good candidate as a target material. AFP has also recently been shown to be at least 50% efficient with NH_3 (researched at UVA Polarized Target Group). More research and development are currently underway. Studies are planned in the near future both for polarized experiments at Jlab as well as the polarized Drell-Yan experiments at Fermilab. Results indicate that as much as 20 minutes could be conserved with every flip cycle, which can add up to considerable overhead for the duration of an experiment.

4.2 Dilution Factors

For the target dilutions studies we will take several different sets of data including empty cell (with ^{4}He/windows/shielding etc.) runs and solid target runs such as ^{12}C and CH_2. Typically, with this target, ^{12}C data is used to approximate the nitrogen contributions. The packing factor and dilutions can be studied with both elastic as well as DIS settings. There were many studies done on the extraction of packing factor/dilution factor from the previous experiments (E143, E155, E155x, GEn-I and GEn-II, RSS and SANE).

References

[1] Belitsky, A.V. and Radyushkin, A.V. Phys.Rept. 418 1-387 (2005)

[2] Berger, Edgar R. and Diehl, M. and Pire, B. Eur. Phys. J. C23 (2002)

[3] Goritschnig, A. T. and Pire, B. and Wagner, J. Phys. Rev. D89 (2014)

[4] Mueller, Dieter and Pire, B. and Szymanowski, L. and Wagner, J. Phys. Rev. D86 031502 (2012)

[5] Moutarde, H. and Pire, B. and Sabatie, F. and Szymanowski, L. and Wagner, J. Phys. Rev. D87 054029 (2013)

[6] Pire, B. and Szymanowski, L. and Wagner, J. Phys. Rev. D83 034009 (2011)

[7] Burkardt, M. and Miller, C.A. and Nowak, W.D. Rept.Prog.Phys. 73 016201 (2010)

[8] Kiptily, D.V. and Polyakov, M.V. Eur. Phys. J. C37 105-114 (2004)

[9]

[10] Courtoy, Aurore and Goldstein, Gary R. and Gonzalez-Hernandez, J. Osvaldo and Liuti, Simonetta and Rajan, Abha Phys. Lett. B731 (2014)

[11] Hatta, Yoshitaka and Yoshida, Shinsuke JHEP 1210 arXiv:hep-ph1207.5332

[12] Boer, M. and Guidal, M. and Vanderhaeghen, M. Eur. Phys. J. A51 8 103 (2015)

[13] Meissner, Stephan and Metz, Andreas and Schlegel, Marc JHEP 0908 056 (2009)

[14] E.R. Berger, M. Diehl, and B. Pire. Timelike compton scattering: exclusive photoproduction of lepton pairs. The European Physical Journal C - Particles and Fields, 23:675689, 2002, hep-ph/0110062

[15] Paremuzyan, R., Timelike Compton Scattering, Ph,D, Thesis, Yerevan, 2010

[16] I. Albayrak et al. (CLAS Collaboration), Jefferson Lab experiment E12-12-001.

[17] Ibrahim H. Albayrak, Timelike Compton Scattering Analysis Note, The Catholic University of America, July, 2013

[18] I. Albayrak et al., Jefferson Lab SoLID experiment E12-12-006A.

[19] JLab proposal PR12-11-108, Spokespersons: K. Allada, J.P. Chen, K. Allada, H. Gao, Z.-E. Meziani

[20] H. Gao *et al.*, EPJ-plus **126**, 2 (2011).

[21] JLab proposal PR-12-09-12 PAC34, PVDIS proposal.

[22] JLab proposal PR-12-09-014, PAC34
http://www.jlab.org/exp_prog/proposals/09/PR12-09-014.pdf.

[23] JLab proposal PR-12-11-007, Spokespersons: J.P. Chen, J, Huang, Y. Qiang, W.B. Yan.

[24] P. Fabbricatore, *et al.* IEEE TRANSACTIONS ON MAGNETICS VOL **32**, NO. 4, 2210 (1996); R. A. Bell, *et al.*, Nucl. Phys. **B78**, 559 (1999).

[25] V. Guzey. Code for cross section calculations for Bethe-Heitler and Timelike Compton Scattering.

[26] D. Crabb *et al.*, Phys. Rev. Lett. **64**, 2627 (1990).

[27] C. Keith *et al.*, NIM A **501**, 327 (2003).

[28] P. Haulte *et al.*, NIM A **356**, 108 (1995).

[29] P. Hautle *et al.* Proceedings of the Workshop on the Polarized Drell-Yan Process, Sante Fe, New Maxico, 2010.

[30] D. Crab, private communications.

[31] W. Anderson *et al.*, arXiv:1103.4277v1 [physics.ins-det].

[32] K. Auki *et al.*, Nucl. Instr. and Meth. A 628 (2011) 300.

[33] B. Azmoun et al., IEEE Trans. Nucl. Sci. 56-3 (2009) 1544.

[34] C. Lu, K.T. McDonald, Nucl. Instr. and Meth. A343 (1994) 135-151.

[35] J. She and B.Q. Ma, Phys. Rev. D **83**, 037502 (2011).

[36] W. Vogelsang and F. Yuan, *private communications.*

[37] H. Avakian *et al.*, a new proposal to PAC38 using a transversely polarized HDiced target.

[38] P. Haulte *et al.*, NIM **A 356**, 108 (1995).